Article:
Cubiss, J. G. orcid.org/0000-0002-5076-8654, Andreyev, A. N. orcid.org/0000-0003-2828-0262, Barzakh, A. E. et al. (48 more authors) (2023) Deformation versus Sphericity in the Ground States of the Lightest Gold Isotopes. Physical Review Letters. 202501. ISSN 1079-7114

https://doi.org/10.1103/PhysRevLett.131.202501

Editors' Suggestion

Deformation versus Sphericity in the Ground States of the Lightest Gold Isotopes

J. G. Cubiss,[1,*] A. N. Andreyev,[1,2] A. E. Barzakh,[3] P. Van Duppen,[4] S. Hilaire,[5] S. Péru,[5] S. Goriely,[6] M. Al Monthery,[1] N. A. Althubiti,[7,8] B. Andel,[9] S. Antalic,[9] D. Atanasov,[10,11] K. Blaum,[10] T. E. Cocolios,[7,4] T. Day Goodacre,[7,11,†] A. de Roubin,[10,‡] G. J. Farooq-Smith,[7,4] D. V. Fedorov,[3] V. N. Fedosseev,[11] D. A. Fink,[11,10] L. P. Gaffney,[4,11,§] L. Ghys,[4,‖] R. D. Harding,[1,11] M. Huyse,[4] N. Imai,[12] D. T. Joss,[13] S. Kreim,[11,10] D. Lunney,[14,¶] K. M. Lynch,[7,11] V. Manea,[10,¶] B. A. Marsh,[11] Y. Martinez Palenzuela,[4,11] P. L. Molkanov,[3] D. Neidherr,[15] G. G. O'Neill,[13] R. D. Page,[13] S. D. Prosnyak,[3] M. Rosenbusch,[16,**] R. E. Rossel,[11,17] S. Rothe,[11,17] L. Schweikhard,[16] M. D. Seliverstov,[3] S. Sels,[4] L. V. Skripnikov,[3] A. Stott,[1] C. Van Beveren,[4] E. Verstraelen,[4] A. Welker,[11,18] F. Wienholtz,[11,16,††] R. N. Wolf,[10,16,‡‡] and K. Zuber[18]

[1]*School of Physics, Engineering and Technology, University of York, York, YO10 5DD, United Kingdom*
[2]*Advanced Science Research Center (ASRC), Japan Atomic Energy Agency, Tokai-mura, Japan*
[3]*Affiliated with an institute covered by a cooperation agreement with CERN*
[4]*KU Leuven, Instituut voor Kern- en Stralingsfysica, 3001 Leuven, Belgium*
[5]*Université Paris-Saclay, CEA, LMCE, 91680, Bruyères-le-Châtel, France*
[6]*Institut d'Astronomie et d'Astrophysique, CP-226, Université Libre de Bruxelles, 1050 Brussels, Belgium*
[7]*The University of Manchester, Department of Physics and Astronomy, Oxford Road, M13 9PL Manchester, United Kingdom*
[8]*Physics Department, College of Science, Jouf University, Sakakah, Kingdom of Saudi Arabia*
[9]*Department of Nuclear Physics and Biophysics, Comenius University in Bratislava, 84248 Bratislava, Slovakia*
[10]*Max-Planck-Institut für Kernphysik, Saupfercheckweg 1, 69117 Heidelberg, Germany*
[11]*CERN, 1211, Geneva 23, Switzerland*
[12]*Center for Nuclear Study (CNS), Graduate School of Science The University of Tokyo, Japan*
[13]*Department of Physics, University of Liverpool, Liverpool, L69 7ZE, United Kingdom*
[14]*CSNSM-CNRS, Université de Paris Sud, 91400 Orsay, France*
[15]*GSI Helmholtzzentrum für Schwerionenforschung GmbH, Darmstadt 64291, Germany*
[16]*Institut für Physik, Universität Greifswald, 17487 Greifswald, Germany*
[17]*Institut für Physik, Johannes Gutenberg-Universität Mainz, Mainz, D-55128, Germany*
[18]*Institut für Kern- und Teilchenphysik, Technische Universität Dresden, Dresden 01069, Germany*

(Received 27 March 2023; revised 2 August 2023; accepted 18 September 2023; published 14 November 2023)

The changes in mean-squared charge radii of neutron-deficient gold nuclei have been determined using the in-source, resonance-ionization laser spectroscopy technique, at the ISOLDE facility (CERN). From these new data, nuclear deformations are inferred, revealing a competition between deformed and spherical configurations. The isotopes ^{180,181,182}Au are observed to possess well-deformed ground states and, when moving to lighter masses, a sudden transition to near-spherical shapes is seen in the extremely neutron-deficient nuclides, ^{176,177,179}Au. A case of shape coexistence and shape staggering is identified in ^{178}Au which has a ground and isomeric state with different deformations. These new data reveal a pattern in ground-state deformation unique to the gold isotopes, whereby, when moving from the heavy to light masses, a plateau of well-deformed isotopes exists around the neutron midshell, flanked by near-spherical shapes in the heavier and lighter isotopes—a trend hitherto unseen elsewhere in the nuclear chart. The experimental charge radii are compared to those from Hartree-Fock-Bogoliubov calculations using the D1M Gogny interaction and configuration mixing between states of different deformation. The calculations are constrained by the known spins, parities, and magnetic moments of the ground states in gold nuclei and show a good agreement with the experimental results.

DOI: 10.1103/PhysRevLett.131.202501

The shape of the atomic nucleus is a result of the interactions between its proton and neutron constituents [1]. At "magic" shell closures, nucleons arrange themselves in energetically stable configurations, producing spherical ground states (except for extreme cases of neutron-proton ratios which form, e.g., the island of inversion [2–6]). However, if one moves just a few nucleons away, residual,

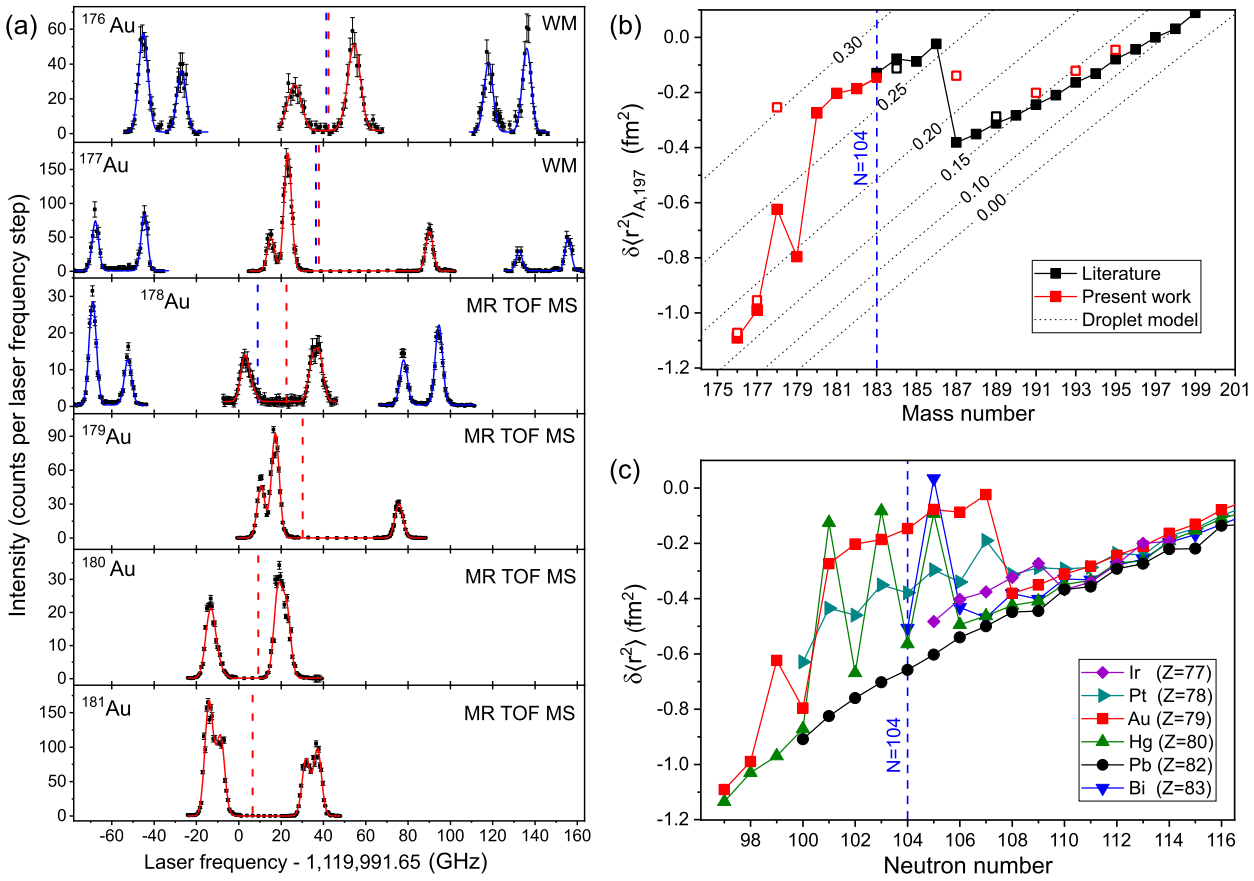

FIG. 1. (a) Examples of hfs spectra collected during the experiment (black data points) fitted with Voigt profiles (solid lines), along with the transition centroid frequencies (vertical dashed lines) and the measuring device used. The red and blue colors represent the fits and centroids for ground and isomeric states and the low- and high-spin states in ^{176}Au, respectively. The y axis is the number of α decays, or the number of ions detected per laser step, in the WM and MR TOF MS, respectively. (b) The $\delta\langle r^2\rangle_{A,197}$ values for gold ground (solid symbols) and isomeric (hollow symbols) states deduced from the IS extracted from the data in (a) (experimental error bars are smaller than the data points). The red and black data points are the results from the present work and literature, respectively [7–13]. The diagonal dotted lines indicate $\delta\langle r^2\rangle_{A,197}$ for fixed deformations predicted by the droplet model ($\langle\beta_2^2\rangle_{\mathrm{DM}}^{1/2}$) [14], using the second parametrization in Ref. [15] and assuming $\beta_2(^{197}\mathrm{Au}) = 0.11$ [9]. The dotted lines are labeled with their corresponding $\langle\beta_2^2\rangle_{\mathrm{DM}}^{1/2}$ values. (c) Comparison of ground-state $\delta\langle r^2\rangle$ values near $N = 104$, for iridium (purple diamond) [16,17], platinum (teal right-pointing triangle) [17–20], gold (red square), mercury (green up-pointing triangle) [21–24], lead (black circle) [25,26], and bismuth (blue down-pointing triangle) [27] isotopes—the chains are arbitrarily offset for the comparison. Error bars are omitted for clarity but are typically smaller than or the same size as the data points.

deformation-driving interactions between valence protons and neutrons come into play. These interactions scale with the number of valence particles, peaking at proton and neutron midshells, where they compete with the stabilizing effects of nearby shell closures. This produces coexisting spherical and deformed structures, creating striking varieties of nuclear shape phenomena.

Characterizing these coexisting structures and their evolution across regions of the nuclear chart is important for furthering our understanding of the governing interactions. In this respect, isotope shift (IS) and hyperfine structure (hfs) measurements, from which changes in nuclear mean-squared charge radii ($\delta\langle r^2\rangle$) and magnetic dipole moments (μ) can be deduced, have proven a powerful tool [28–30]. While μ provides insight into the orbitals occupied by unpaired nucleons, the $\delta\langle r^2\rangle$ value is sensitive to the radial charge distribution of the nucleus and, hence, to changes in its shape.

The nuclei surrounding the $Z = 82$ shell closure have been the focus of an extensive campaign of such IS and hfs measurements and display some of the best-known examples of nuclear shape coexistence. Notably, while the ground states of semimagic lead nuclei remain near spherical [25,26], those of the mercury ($Z = 80$) [21–24] and the bismuth ($Z = 83$) [27] isotopic chains are seen to stagger dramatically between strongly deformed and near-spherical shapes around the $N = 104$ neutron midshell, where a strong competition between coexisting spherical and prolate configurations takes place. Above $Z = 82$, departures from spherical ground states are observed in

the polonium ($Z = 84$) [31,32] and astatine ($Z = 85$) isotopes [33], with smooth but rapid onsets of deformation occurring when moving away from $N = 126$. Meanwhile, below the proton shell closure, spherical ground states coexist with low-lying, deformed isomers in the thallium ($Z = 81$) chain [34,35].

In this work, we present our results from IS and hfs measurements for neutron-deficient gold ($Z = 79$) nuclides, using the in-source, resonant-ionization laser spectroscopy technique. The study was performed at the ISOLDE facility in CERN, for which partial results for the nuclear spin (I), μ values, and decay properties of some gold isotopes have been presented [36–41]. Previous IS studies of gold isotopes found a remarkable transition from near-spherical ground states in $^{187–199}$Au ($N = 108$–120), to strongly deformed, presumably prolate configurations in $^{183–186}$Au ($N = 104$–107) [7–13]. However, questions remain; What happens to the ground states in the lightest isotopes of gold? Do they remain strongly deformed, or do they return toward sphericity? This Letter will answer these questions.

The gold nuclei were produced in spallation reactions induced by impinging a beam of protons with an energy of 1.4 GeV and a maximum current of 2.1 μA, onto a 50 g/cm^2 UC_x target. After proton impact, reaction products diffused out of the target matrix and effused toward a hot cavity ion source [42], kept at a temperature of ≈2300 K. Inside the cavity, gold isotopes were selectively ionized using the three-step ionization scheme shown in Fig. 1 in [43] (see also Supplemental Material [44]). The ions were extracted by a 30 kV potential and mass separated by the ISOLDE general purpose separator (GPS) [51], before transportation to either the windmill (WM) system [52,53] or ISOLTRAP's [54] multireflection time-of-flight mass spectrometer (MR TOF MS) [55] for ion counting. To construct hfs spectra, the number of characteristic alpha or gamma decays measured in the WM or of mass-resolved ions of interest detected by the MR TOF MS were recorded for each frequency step (see Ref. [33] for details). The IS measurements were made by scanning the 267.6 nm atomic transition ($6s^2S_{1/2} \rightarrow 6p^2P^o_{1/2}$), using a frequency-tripled titanium sapphire laser operated in a narrow-band mode (≈600 MHz bandwidth before frequency tripling), with the laser wavelength recorded using a high-finesse/Angstrom WS7 wave meter. References for the IS measurements were made regularly, using a Faraday cup to record hfs spectra of stable ^{197}Au.

Examples of the measured hfs spectra are shown in Fig. 1(a). Voigt profiles are fitted to the different components, with positions determined by the standard relation [28] and intensities using the procedure described in Ref. [53] (see Supplemental Material [44] for further details). The fits were made assuming fixed I values taken from available data [56] and our previous studies [36–41], while the IS relative to stable ^{197}Au ($\delta\nu_{A,197} = \nu_A - \nu_{197}$) and the magnetic hfs constants for the atomic levels of the scanned transition (a_{6s} and a_{6p}) were left as free parameters.

The measured $\delta\nu_{A,197}$ value is related to the $\delta\langle r^2\rangle_{A,197}$ via $\delta\nu_{A,197} = (k_{\mathrm{NMS}} + k_{\mathrm{SMS}})[(1/M_A) - (1/M_{197})] + \mathcal{F}\delta\langle r^2\rangle_{A,197}$, where the field shift constant $\mathcal{F}$ and the normal (k_{NMS}) and specific (k_{SMS}) mass shift constants needed to be calculated and M_A is the atomic mass of the isotope with mass number A.

For this work, new atomic physics calculations have been performed employing relativistic coupled cluster theory, using the Dirac-Coulomb Hamiltonian, with a correction on the Gaunt interelectron interaction. Up to perturbative quadruple cluster amplitudes are taken into account for the correlation treatment, which is quite new for IS problems [57–61]. The constants k_{NMS} and k_{SMS} are calculated using fully relativistic operators [44,62–65]. In the calculations, the locally modified relativistic electronic structure codes [66–75] have been used as well as our method of constructing compact basis sets [59,76]. The results give $\mathcal{F} = -40.1(11)$ GHz/fm^2, $k_{\mathrm{NMS}} = 600(40)$ GHz u, and $k_{\mathrm{SMS}} = 103(93)$ GHz u, giving a total mass shift constant is $k_{\mathrm{NMS}} + k_{\mathrm{SMS}} = 703(101)$ GHz u.

Our $\delta\nu_{A,197}$ and corresponding $\delta\langle r^2\rangle_{A,197}$ results for gold nuclei are given in Table I. The accompanying $\langle\beta_2^2\rangle^{1/2}_{\mathrm{DM}}$ values are root-mean-squared deformation parameters based on comparison of our $\delta\langle r^2\rangle_{A,197}$ values with droplet model (DM) predictions, using the second parametrization in Ref. [15] and assuming $\beta_2(^{197}\mathrm{Au}) = 0.11$ [9].

Our new $\delta\langle r^2\rangle_{A,197}$ values are plotted in Fig. 1(b), along with literature values for $^{183–199}$Au taken from [9–11,13,39]. The literature values display a large jump in deformation at ^{186}Au, followed by a plateau of strongly deformed ground states for $^{183–186}$Au, extending down to $N = 104$. Our results show that this plateau continues down to ^{180}Au, with a large and sudden step back toward sphericity at ^{179}Au ($N = 100$). Apart from ^{178}Au^{g,m}, which display a case for shape coexistence and shape staggering relative to their spherical neighbors [77], the lightest gold isotopes evolve toward near sphericity, down to the extremely neutron-deficient case ^{176}Au ($N = 97$).

In Fig. 1(c), we compare the $\delta\langle r^2\rangle$ for ground states of gold, bismuth, mercury, iridium, and platinum nuclides (isomeric states are omitted for clarity) to those of the spherical lead isotopes. The data for thallium ground states are not included here, as they follow the same trend as the lead isotopes (see Refs. [34,35]). The gold, mercury, and bismuth chains display dramatic changes in ground-state deformation relative to the lead nuclides around $N = 104$, with large increases in $\delta\langle r^2\rangle$ indicating sudden transitions from near-spherical to strongly deformed configurations. Though the staggering patterns in the mercury and bismuth

TABLE I. Values for the IS ($\delta\nu_{A,197}$) and $\delta\langle r^2\rangle_{A,197}$ relative to ^{197}Au extracted from the experimental data, assuming different I assignments. The I values in parentheses represent cases where the assignment is not certain or has not been directly measured. Statistical uncertainties from fits to the data are given in round parentheses, while systematic uncertainties stemming from the atomic calculations are given in curly brackets. The $\langle\beta_2^2\rangle_{\rm DM}^{1/2}$ values are taken from comparison to predictions from the DM. Our values of $\mu(^{181,183}\mathrm{Au})$ are presented here for the first time, while the other values are included for completeness—all μ values are calculated taking the hyperfine anomaly into account as described in [41].

Isotope	I	$\delta\nu_{A,197}$ (MHz)	$\delta\langle r^2\rangle_{A,197}$ (fm^2)	$\langle\beta_2^2\rangle_{\rm DM}^{1/2}$	μ (μ_N)
^{176}Au^{ls}	(3)	43340(640)	−1.091(16){31}	0.17	−0.823(48) [40]
	(4)	42860(660)	−1.079(16){31}	0.17	−0.853(54) [40]
	(5)	42520(700)	−1.071(16){31}	0.17	−0.873(55) [40]
^{176}Au^{hs}	(8)	42580(310)	−1.072(8){31}	0.17	5.14(20) [40]
	(9)	43070(370)	−1.085(9){31}	0.17	5.18(20) [40]
^{177}Au^{g}	1/2	39290(220)	−0.990(5){29}	0.18	1.257(64)[a]
^{177}Au^{m}	(11/2)	37860(250)	−0.954(6){28}	0.19	6.519(38) [41]
^{178}Au^{g}	(2)	24650(260)	−0.624(7){18}	0.24	−0.884(68) [38]
	(3)	23800(260)	−0.603(7){18}	0.25	−0.962(77) [38]
^{178}Au^{m}	(7)	9790(140)	−0.254(3){8}	0.30	4.84(8) [38]
	(8)	10300(140)	−0.266(3){9}	0.30	4.89(8) [38]
^{179}Au	1/2	31570(200)	−0.796(5){23}	0.19	1.050(30)[a]
^{180}Au	(1)	10650(200)	−0.274(5){9}	0.28	−0.830(90) [37]
^{181}Au	(3/2)	7820(230)	−0.203(6){7}	0.28	1.238(67)[b]
^{182}Au	(2)	7160(200)	−0.186(5){6}	0.27	1.664(91) [37]
^{183}Au	(5/2)	5620(120)	−0.147(3){5}[c]	0.27	2.057(39)[d]
^{187}Au^{m}	(9/2)	5380(160)	−0.139(4){4}[e]	0.23	3.529(53) [39]
^{191}Au^{m}	(11/2)	7950(180)	−0.201(4){6}	0.16	6.326(37) [41]
^{193}Au^{m}	11/2	4780(180)	−0.121(4){4}	0.15	6.320(37) [41]
^{195}Au^{m}	11/2	1760(220)	−0.045(5){1}	0.13	6.316(37) [41]

[a]Recalculated from the experimental hfs a constants from [36].
[b]Derived from experimental data $a_{6s} = 22900(100)$ MHz, $a_{6p}/a_{6s} = 0.1155(45)$ (present work).
[c]Our value differs to $\delta\langle r^2\rangle_{A,197}(^{183}\mathrm{Au}) = -0.130(9)$ [10], partially due to the different electronic factors used.
[d]Derived from experimental data $a_{6s} = 23037(40)$ MHz, $a_{6p}/a_{6s} = 0.1148(15)$ (present work). The small difference between ours and the literature value of $1.972(23)\mu_N$ [10] is due to the treatment of the hyperfine anomaly.
[e]$\delta\langle r^2\rangle_{A,197}(^{187}\mathrm{Au}^m)$ is calculated using the new electronic factors, with $\delta\nu_{A,197}(^{187}\mathrm{Au}^m)$ taken from [39].

radii bear a resemblance, the trend followed by the gold nuclei is notably different. Here, similar to the platinum and iridium isotopes, the increase in $\delta\langle r^2\rangle$ values around $N = 104$ indicates a transition to deformed ground-state configurations for both the odd- and even-N gold isotopes. However, the observed step in the charge radii in the gold chain is significantly larger than that in the platinum and iridium cases. Furthermore, the transition from spherical to strongly deformed shapes is much sharper in the gold compared to that seen in the platinum chain, and, while a prominent odd-even staggering is observed in the latter, the trend followed by the strongly deformed gold cases is much flatter. This sharp and large jump between near-spherical ground states, to a plateau of strongly deformed ones at the neutron midshell, is a pattern that is unique to the gold isotopes within the chart of nuclides.

As well as $\delta\langle r^2\rangle_{A,197}$ values, Table I gives values for μ, most of which were published in our previous works [36–41] but are included for completeness. All μ values have been calculated using the approach to the hyperfine anomaly (hfa) described in [41], including $\mu(^{177,179}\mathrm{Au})$ which have been recalculated from [36]. Our value for $\mu(^{83}\mathrm{Au})$ agrees reasonably with $\mu(^{183}\mathrm{Au}) = 1.972(23)\mu_N$ [10], with the small difference due to the different treatment of the hfa. Our new result for ^{181}Au assumes $I = 3/2$, which gives an experimental μ in good agreement with that expected of a single-particle $\pi h_{9/2}$ state ($\mu_{\rm eff}(\pi h_{9/2}) = 1.185$, using an effective spin g factor $g_{s,\rm eff} = 0.6 g_s$).

To further explore our experimental results, we have performed Hartree-Fock-Bogoliubov (HFB) calculations following the protocol of Ref. [78]. The candidates for the empirical ground states are chosen from the calculations for having (i) the same I^π as that assigned experimentally; (ii) the value of μ in best agreement with the experimental data; and (iii) an excitation energy of < 1 MeV relative to the theoretical ground state. Note that similar selection criteria were recently used successfully for modeling the radii of mercury isotopes using the Monte Carlo shell model (MCSM) [23,24]. However, odd-odd nuclei such as those in the gold chain remain a challenge for the MCSM approach.

Our HFB calculations use the D1M Gogny interaction [79] with the equal filling approximation for the odd-A and odd-odd gold nuclei. Similarly to our recent works [27,78,80,81], potential energy surfaces are calculated while blocking quasiparticles that are compatible with the I^π for the ground and isomeric states deduced from experiment, and, for ^{183,185}Au, the known $K^\pi = 1/2^-$ assignments were used (see Ref. [82] and references therein).

Magnetic moments are calculated with the method described in Ref. [78], using an effective operator $\hat{\mu}^{\rm eff} = 0.82 g_s \hat{s} + 1.25 g_\ell \hat{\ell}$, where g_ℓ is the orbital g factor for the free nucleon. Effective coefficients are used to account for beyond mean-field and core-polarization effects [83], which are required to reproduce experimental values. For strongly deformed cases, rotational contributions are also included.

The calculated and experimental $\delta\langle r^2\rangle_{A,197}$ values for gold isotopes are compared in Fig. 2 (a similar comparison for μ is provided in Supplemental Material [44]). The main features of the experimental results are reproduced well: moving from heavier to lighter masses, the jump from near-spherical to well deformed at $A = 186$; a retention of

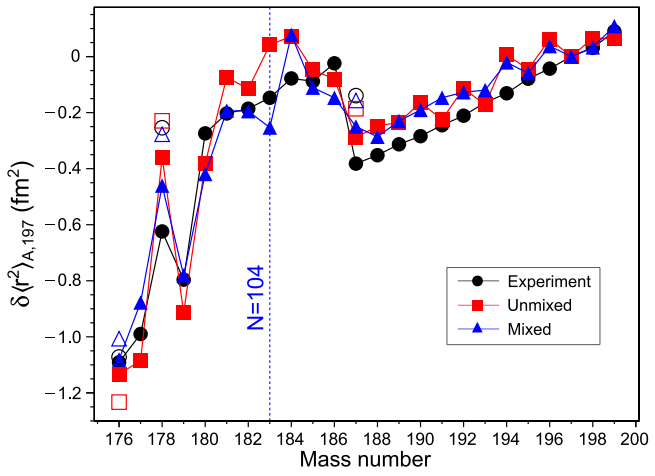

FIG. 2. Comparison between experimental $\delta\langle r^2\rangle_{A,197}$ values (black circle) for gold isotopes with HFB calculations without (red square) and with (blue up-pointing triangle) CM included. The filled symbols connected by lines indicate ground states, while the hollow symbols represent the isomers in ^{178,187}Au and the high-spin state in ^{176}Au. The $11/2^-$ isomers have been excluded for clarity.

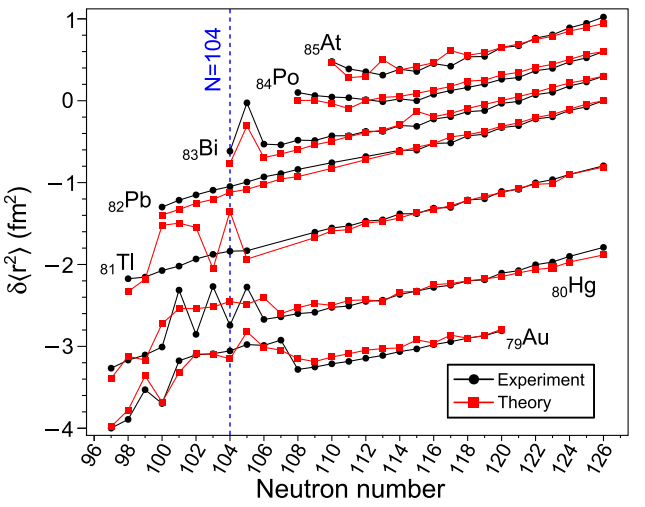

FIG. 3. Comparison between experimental (black circle) and theoretical (red square) results for ground-state $\delta\langle r^2\rangle$ values along isotopic chains. The isotopic chains are arbitrarily offset from each other for clarity and are labeled with their chemical symbol and proton number.

strongly deformed ground states for $A = 180$–186; a return toward sphericity for ^{176,177,179}Au; and the shape staggering and large isomer shift in ^{178}Au.

However, at points, there remain discrepancies between experiment and theory which may be due to configuration mixing (CM) between states of different deformation, as was recently seen in the bismuth isotopes [27]. The possible influence of CM in the gold isotopes was explored following the same method used in Ref. [27], taken from statistical physics [84,85]. Here, several states of different deformations (q) are mixed, and the average value of an observable ($\mathcal{O}$) is calculated using the expression

$$\langle\mathcal{O}\rangle = \frac{\int \mathcal{O}\exp[E(q)/T]dq}{\int \exp[E(q)/T]dq}, \quad (1)$$

where $E(q)$ is the HFB energy of the potential energy surface at deformation q and T is a parameter which allows mixing between low-lying states. For our calculations, a value of $T = 0.5$ MeV was used.

The calculated results including CM are shown in Fig. 2. An improved agreement is observed in the region of strong ground-state deformation, while the description of the near-spherical cases remains comparable to those without CM. Overall, though differences remain, a good agreement between experiment and calculation is observed, especially considering the odd-A and odd-odd nature of gold isotopes.

The general applicability of our approach was investigated by performing calculations for neutron-deficient nuclei from mercury ($Z = 80$) to astatine ($Z = 85$). These nuclides are a hotbed of shape phenomena, transitioning from the staggering in ground-state deformation of the mercury isotopes that lie below spherical lead nuclei [25,26] to the polonium [31,32] and astatine nuclides [33] with their early onsets of deformation as the neutron number moves away from $N = 126$. All of this comes in addition to the cases of shape coexistence that are commonplace throughout this region. This variety in behavior poses a significant challenge to any theoretical approach, particularly when attempting to tackle them in a consistent manner.

For these calculations CM was included, and the same I^π, μ, and excitation energy (< 1 MeV) selection criteria were used. The results are compared to experimental data in Fig. 3. A good overall agreement is seen across the region; however, there are large discrepancies between for some thallium and mercury isotopes. For the former, strong deformations are calculated in a number of the lightest isotopes that are known to have near-spherical shapes, while for the latter, the dramatic staggering is not reproduced.

Closer inspection of the calculations for thallium isotopes show that, when a state with strong deformation is selected, it has only a fractionally better μ relative to experiment than a spherical candidate. Thus, our selection criteria do not work in these particular cases. For the mercury chain, it was shown in Ref. [78] that the staggering was reproducible only by selecting states in the even-even isotopes with correct deformations. In our calculations, the staggering can be reproduced only if an extra constraint on the $\delta\langle r^2\rangle$ is used for state selection (see Supplemental Material [44]). This indicates that there are candidates present at low excitation energies in the HFB calculations with a set of properties consistent with experimental data; however, the present ingredients of the D1M Gogny interaction are not sufficient to correctly predict them as ground states.

In summary, the $\delta\langle r^2\rangle$ values of ground and isomeric states in neutron-deficient gold isotopes have been measured using the in-source, resonant-ionization technique. Advanced atomic calculations of the electronic factors with the refined correlation treatment enable us to decrease systematic theoretical uncertainties in $\delta\langle r^2\rangle$ down to 2.7%, which is comparable in many cases to the experimental uncertainties. An end to the region of strongly deformed ground states has been observed, and a move toward sphericity is seen in ^{176,177,179}Au. Our results reveal a unique pattern in the ground-state shape evolution of gold isotopes that so far has not been observed elsewhere in the nuclear chart.

HFB calculations were performed for gold isotopes using the D1M Gogny interaction and a schematic approach to CM between states of different deformations, with the experimental μ and I^π used as criteria for selecting candidate states. A good agreement between these calculations and experimental results was obtained. Further $\delta\langle r^2\rangle$ calculations were performed for the ground states of neutron-deficient nuclides near $Z = 82$. A good agreement with experiment was observed, with candidates for ground states with correct I^π and μ values found for almost all cases across the region. However, the criteria needed for selecting appropriate states from the calculations highlight that further refinement of the present interaction is required. In this respect, $\delta\langle r^2\rangle$ and μ values can play an important role in constraining the development of future interactions. In addition, though the schematic statistical approach toward CM used was successful, it indicates the necessity to include such mixing at a microscopic level in the future works.

We acknowledge the support of the ISOLDE Collaboration and technical teams. This work was done with support from European Union's Seventh Framework Program for Research and Technological Development under Grant Agreements No. 262010 (ENSAR), No. 267194 (COFUND), and No. 289191 (LA3NET), from the European Union's Horizon 2020 Framework research and innovation program under Grant Agreement No. 654002 (ENSAR2), from grants by the United Kingdom Science and Technology Facilities Council Grants No. ST/P003885/1, No. ST/P004598/1, and No. ST/V001027/1 from the BMBF (05P12HGCI1, 05P15ODCIA, 05P15HGCIA, 05P18HGCIA, and 05P21HGCI1), from the Max Planck Society, from the French IN2P3, for funding received from Research Foundation Flanders (FWO, Belgium), by GOA/2015/010 (BOF KU Leuven) and the FWO and F. R. S.-FNRS under the Excellence of Science (EOS) program (40007501), from the Slovak Research and Development Agency (Contract No. APVV-18-0268) and the Slovak Grant Agency VEGA (Contract No. 1/0651/21). A. W. acknowledges support by a Wolfgang Gentner Ph.D. scholarship of the BMBF (05E15CHA).

*james.cubiss@york.ac.uk
†Present address: TRIUMF, Vancouver, BC V6T 2A3, Canada.
‡Present address: Centre d'Etudes Nucléaires de Bordeaux-Gradignan, 19 Chemin du Solarium, CS 10120, F-33175 Gradignan, France.
§Present address: Department of Physics, University of Liverpool, Liverpool, L69 7ZE, United Kingdom.
‖Present address: Belgian Nuclear Research Center SCK CEN, Boeretang 200, B-2400 Mol, Belgium.
¶Present address: Université Paris-Saclay, CNRS/IN2P3, IJCLab, 91405 Orsay, France.
**Present address: RIKEN Nishina Center for Accelerator-Based Science, Wako, Saitama 351-0198, Japan.
††Present address: Institut für Kernphysik, Technische Universität Darmstadt, 64289 Darmstadt, Germany.
‡‡Present address: ARC Centre of Excellence for Engineered Quantum Systems, The University of Sydney, NSW 2006, Australia.

[1] K. Heyde and J. L. Wood, Rev. Mod. Phys. **83**, 1467 (2011).
[2] C. Thibault, R. Klapisch, C. Rigaud, A. M. Poskanzer, R. Prieels, L. Lessard, and W. Reisdorf, Phys. Rev. C **12**, 644 (1975).
[3] A. Poves and J. Retamosa, Phys. Lett. B **184**, 311 (1987).
[4] E. K. Warburton, J. A. Becker, and B. A. Brown, Phys. Rev. C **41**, 1147 (1990).
[5] G. Neyens, M. Kowalska, D. Yordanov, K. Blaum, P. Himpe, P. Lievens, S. Mallion, R. Neugart, N. Vermeulen, Y. Utsuno, and T. Otsuka, Phys. Rev. Lett. **94**, 022501 (2005).
[6] D. T. Yordanov, M. Kowalska, K. Blaum, M. De Rydt, K. T. Flanagan, P. Lievens, R. Neugart, G. Neyens, and H. H. Stroke, Phys. Rev. Lett. **99**, 212501 (2007).
[7] C. Ekström, L. Robertsson, S. Ingelman, G. Wannberg, and I. Ragnarsson, Nucl. Phys. **A348**, 25 (1980).
[8] K. Wallmeroth, G. Bollen, A. Dohn, P. Egelhof, J. Grüner, F. Lindenlauf, U. Krönert, J. Campos, A. Rodriguez Yunta, M. J. G. Borge, A. Venugopalan, J. L. Wood, R. B. Moore, and H. J. Kluge, Phys. Rev. Lett. **58**, 1516 (1987).
[9] K. Wallmeroth, G. Bollen, A. Dohn, P. Egelhof, U. Krönert, M. J. G. Borge, J. Campos, A. R. Yunta, K. Heyde, C. De Coster, J. L. Wood, and H. J. Kluge, Nucl. Phys. **A493**, 224 (1989).
[10] U. Krönert, S. Becker, G. Bollen, M. Gerber, T. Hilberath, H. J. Kluge, and G. Passler, Z. Phys. A At. Nucl. **331**, 521 (1988).
[11] G. Savard, J. Crawford, J. Lee, G. Thekkadath, H. Duong, J. Pinard, F. Le Blanc, P. Kilcher, J. Obert, J. Oms, J. Putaux, B. Roussiere, and J. Sauvage, Nucl. Phys. **A512**, 241 (1990).
[12] G. Passler, J. Rikovska, E. Arnold, H.-J. Kluge, L. Monz, R. Neugart, H. Ravn, and K. Wendt, Nucl. Phys. **A580**, 173 (1994).
[13] F. Le Blanc, J. Obert, J. Oms, J. C. Putaux, B. Roussière, J. Sauvage, J. Pinard, L. Cabaret, H. T. Duong, G. Huber, M. Krieg, V. Sebastian, J. Crawford, J. K. P. Lee, J. Genevey, and F. Ibrahim, Phys. Rev. Lett. **79**, 2213 (1997).
[14] W. D. Myers and K. H. Schmidt, Nucl. Phys. **A410**, 61 (1983).
[15] D. Berdichevsky and F. Tondeur, Z. Phys. A At. Nucl. **322**, 141 (1985).

[16] D. Verney *et al.*, Eur. Phys. J. A **30**, 489 (2006).
[17] I. Angeli and K. P. Marinova, At. Data Nucl. Data Tables **99**, 69 (2013).
[18] T. Hilberath, S. Becker, G. Bollen, H. J. Kluge, U. Kronert, G. Passler, J. Rikovska, and R. Wyss, Z. Phys. A Hadrons Nucl. **342**, 1 (1992).
[19] F. Le Blanc, Hyperfine Interact. **127**, 71 (2000).
[20] J. Sauvage *et al.*, Hyperfine Interact. **129**, 303 (2000).
[21] J. Bonn, G. Huber, H. J. Kluge, L. Kugler, and E. W. Otten, Phys. Lett. B **38**, 308 (1972).
[22] G. Ulm, S. K. Bhattacherjee, P. Dabkiewicz, G. Huber, H. J. Kluge, T. Kühl, H. Lochmann, E. W. Otten, K. Wendt, S. A. Ahmad, W. Klempt, and R. Neugart, Z. Phys. A At. Nucl. **325**, 247 (1986).
[23] B. A. Marsh *et al.*, Nat. Phys. **14**, 1163 (2018).
[24] S. Sels *et al.*, Phys. Rev. C **99**, 044306 (2019).
[25] H. De Witte *et al.*, Phys. Rev. Lett. **98**, 112502 (2007).
[26] M. D. Seliverstov *et al.*, Eur. Phys. J. A **41**, 315 (2009).
[27] A. Barzakh *et al.*, Phys. Rev. Lett. **127**, 192501 (2021).
[28] E. W. Otten, in *Treatise on Heavy Ion Science*, 1st ed., edited by D. A. Bromley (Springer US, Boston, MA, 1989), Chap. 7, pp. 517–638, 10.1007/978-1-4613-0713-6_7.
[29] B. Cheal and K. T. Flanagan, J. Phys. G **37**, 113101 (2010).
[30] P. Campbell, I. Moore, and M. Pearson, Prog. Part. Nucl. Phys. **86**, 127 (2016).
[31] T. E. Cocolios *et al.*, Phys. Rev. Lett. **106**, 052503 (2011).
[32] M. D. Seliverstov *et al.*, Phys. Lett. B **719**, 362 (2013).
[33] J. G. Cubiss *et al.*, Phys. Rev. C **97**, 054327 (2018).
[34] A. E. Barzakh, L. K. Batist, D. V. Fedorov, V. S. Ivanov, K. A. Mezilev, P. L. Molkanov, F. V. Moroz, S. Y. Orlov, V. N. Panteleev, and Y. M. Volkov, Phys. Rev. C **88**, 024315 (2013).
[35] A. E. Barzakh *et al.*, Phys. Rev. C **95**, 014324 (2017).
[36] J. G. Cubiss *et al.*, Phys. Lett. B **786**, 355 (2018).
[37] R. D. Harding *et al.*, Phys. Rev. C **102**, 024312 (2020).
[38] J. G. Cubiss *et al.*, Phys. Rev. C **102**, 044332 (2020).
[39] A. E. Barzakh *et al.*, Phys. Rev. C **101**, 064321 (2020).
[40] R. D. Harding *et al.*, Phys. Rev. C **104**, 024326 (2021).
[41] A. E. Barzakh *et al.*, Phys. Rev. C **101**, 034308 (2020).
[42] V. I. Mishin, V. N. Fedoseyev, H.-J. Kluge, V. S. Letokhov, H. L. Ravn, F. Scheerer, Y. Shirakabe, S. Sundell, and O. Tengblad, Nucl. Instrum. Methods Phys. Res., Sect. B **73**, 550 (1993).
[43] B. A. Marsh, V. N. Fedosseev, and P. Kosuri, Hyperfine Interact. **171**, 109 (2006).
[44] See Supplemental Material at http://link.aps.org/supplemental/10.1103/PhysRevLett.131.202501, for more information on the atomic calculations, which include Refs. [45–50].
[45] K. Heilig and A. Steudel, At. Data Nucl. Data Tables **14**, 613 (1974).
[46] M. Kállay and J. Gauss, J. Chem. Phys. **123**, 214105 (2005).
[47] K. G. Dyall, Theor. Chem. Acc. **115**, 441 (2006).
[48] K. G. Dyall, Theor. Chem. Acc. **99**, 366 (1998).
[49] L. Visscher, T. J. Lee, and K. G. Dyall, J. Chem. Phys. **105**, 8769 (1996).
[50] R. J. Bartlett and M. Musiał, Rev. Mod. Phys. **79**, 291 (2007).
[51] E. Kugler, Hyperfine Interact. **129**, 23 (2000).
[52] A. N. Andreyev *et al.*, Phys. Rev. Lett. **105**, 252502 (2010).
[53] M. D. Seliverstov *et al.*, Phys. Rev. C **89**, 034323 (2014).
[54] M. Mukherjee, D. Beck, K. Blaum, G. Bollen, J. Dilling, S. George, F. Herfurth, A. Herlert, A. Kellerbauer, H. J. Kluge, S. Schwarz, L. Schweikhard, and C. Yazidjian, Eur. Phys. J. A **35**, 1 (2008).
[55] R. N. Wolf, F. Wienholtz, D. Atanasov, D. Beck, K. Blaum, C. Borgmann, F. Herfurth, M. Kowalska, S. Kreim, Y. A. Litvinov, D. Lunney, V. Manea, D. Neidherr, M. Rosenbusch, L. Schweikhard, J. Stanja, and K. Zuber, Int. J. Mass Spectrom. **349–350**, 123 (2013).
[56] From ENSDF database as of October 9th, 2023. Version available at, http://www.nndc.bnl.gov/ensarchivals/.
[57] G. Penyazkov, S. D. Prosnyak, A. E. Barzakh, and L. V. Skripnikov, J. Chem. Phys. **158**, 114110 (2023).
[58] S. D. Prosnyak and L. V. Skripnikov, Phys. Rev. C **103**, 034314 (2021).
[59] L. V. Skripnikov, J. Chem. Phys. **153**, 114114 (2020).
[60] S. D. Prosnyak, D. E. Maison, and L. V. Skripnikov, J. Chem. Phys. **152**, 044301 (2020).
[61] L. V. Skripnikov, A. V. Titov, and V. V. Flambaum, Phys. Rev. A **95**, 022512 (2017).
[62] V. M. Shabaev, Theor. Math. Phys. **63**, 588 (1985).
[63] C. W. P. Palmer, J. Phys. B **20**, 5987 (1987).
[64] V. M. Shabaev, Sov. J. Nucl. Phys. **47**, 69 (1988).
[65] V. Shabaev and A. Artemyev, J. Phys. B **27**, 1307 (1994).
[66] DIRAC, a relativistic *ab initio* electronic structure program, release DIRAC15 (2015), written by R. Bast, T. Saue, L. Visscher, and H. J. Aa. Jensen, with contributions from V. Bakken, K. G. Dyall, S. Dubillard, U. Ekstroem, E. Eliav, T. Enevoldsen, E. Fasshauer, T. Fleig, O. Fossgaard, A. S. P. Gomes, T. Helgaker, J. Henriksson, M. Ilias, Ch. R. Jacob, S. Knecht, S. Komorovsky, O. Kullie, J. K. Laerdahl, C. V. Larsen, Y. S. Lee, H. S. Nataraj, M. K. Nayak, P. Norman, G. Olejniczak, J. Olsen, Y. C. Park, J. K. Pedersen, M. Pernpointner, R. Di Remigio, K. Ruud, P. Salek, B. Schimmelpfennig, J. Sikkema, A. J. Thorvaldsen, J. Thyssen, J. van Stralen, S. Villaume, O. Visser, T. Winther, and S. Yamamoto (see http://www.diracprogram.org).
[67] R. Saue *et al.*, J. Chem. Phys. **152**, 204104 (2020).
[68] M. Kállay, P. R. Nagy, D. Mester, Z. Rolik, G. Samu, J. Csontos, J. Csóka, P. B. Szabó, L. Gyevi-Nagy, B. Hégely, I. Ladjánszki, L. Szegedy, B. Ladóczki, K. Petrov, M. Farkas, P. D. Mezei, and á. Ganyecz (MRCC), The MRCC program system: Accurate quantum chemistry from water to proteins, J. Chem. Phys. **152**, 074107 (2020). MRCC, a quantum chemical program suite written by M. Kállay, P. R. Nagy, D. Mester, Z. Rolik, G. Samu, J. Csontos, J. Csóka, P. B. Szabó, L. Gyevi-Nagy, B. Hégely, I. Ladjánszki, L. Szegedy, B. Ladóczki, K. Petrov, M. Farkas, P. D. Mezei, and á. Ganyecz. See http://www.mrcc.hu.
[69] M. Kállay and P. R. Surján, J. Chem. Phys. **115**, 2945 (2001).
[70] M. Kállay, P. G. Szalay, and P. R. Surján, J. Chem. Phys. **117**, 980 (2002).
[71] A. V. Oleynichenko, A. Zaitsevskii, and E. Eliav, in *Supercomputing*, edited by V. Voevodin and S. Sobolev (Springer International Publishing, Cham, 2020), Vol. 1331, pp. 375–386, 10.1007/978-3-030-64616-5_33.
[72] A. Oleynichenko, A. Zaitsevskii, and E. Eliav (2021), EXP-T, an extensible code for Fock space relativistic

coupled cluster calculations (see http://www.qchem.pnpi.spb.ru/expt) (accessed on 4 February 2022).
[73] I. I. Tupitsyn, G. B. Deyneka, and V. F. Bratzev, HFD (1977–2002), HFD, a program for atomic finite-difference four-component Dirac-Hartree-Fock calculations on the base of the HFD code [75].
[74] I. I. Tupitsyn, HFDB (2003), HFDB, a program for atomic finite-difference four-component Dirac-Hartree-Fock-Breit calculations written on the base of the HFD code [75].
[75] V. F. Bratzev, G. B. Deyneka, and I. I. Tupitsyn, Bull. Acad. Sci. USSR, Phys. Ser. (English Transl.) **41**, 173 (1977).
[76] L. V. Skripnikov, N. S. Mosyagin, and A. V. Titov, Chem. Phys. Lett. **555**, 79 (2013).
[77] The large increase in deformation for $^{178}\mathrm{Au}^{m}$ relative to $^{178}\mathrm{Au}^{g}$ and heavier gold isotopes is related to the occupation of a different proton orbital. As discussed in [38], the last proton in $^{178}\mathrm{Au}^{m}$ occupies a $9/2[514]_{h_{11/2}}$ orbital, whereas for all other strongly deformed cases ($^{178}\mathrm{Au}^{g}$ included) it is in either a $1/2[541]_{h_{9/2}}$ or $3/2[532]_{h_{9/2}}$ state.
[78] S. Péru, S. Hilaire, S. Goriely, and M. Martini, Phys. Rev. C **104**, 024328 (2021).
[79] S. Goriely, S. Hilaire, M. Girod, and S. Péru, Phys. Rev. Lett. **102**, 242501 (2009).
[80] T. Day Goodacre *et al.*, Phys. Rev. Lett. **126**, 032502 (2021).
[81] T. Day Goodacre *et al.*, Phys. Rev. C **104**, 054322 (2021).
[82] C. R. Bingham, M. B. Kassim, M. Zhang, Y. A. Akovali, K. S. Toth, W. D. Hamilton, H. K. Carter, J. Kormicki, J. Von Schwarzenberg, and M. M. Jarrio, Phys. Rev. C **51**, 125 (1995).
[83] A. Arima, Sci. China Phys. Mech. Astron. **54**, 188 (2011).
[84] V. Martin, J. L. Egido, and L. M. Robledo, Phys. Rev. C **68**, 034327 (2003).
[85] S. Hilaire, M. Girod, S. Goriely, and A. J. Koning, Phys. Rev. C **86**, 064317 (2012).